

A compact neuromorphic system for ultra energy-efficient, on-device robot localization

Adam D Hines^{1*}, Michael Milford¹, Tobias Fischer¹

¹QUT Centre for Robotics, Queensland University of Technology,
2 George St, Brisbane, QLD 4001, Australia

*To whom correspondence should be addressed; E-mail: adam.hines@qut.edu.au

Neuromorphic computing offers a transformative pathway to overcome the computational and energy challenges faced in deploying robotic localization and navigation systems at the edge. Visual place recognition, a critical component for navigation, is often hampered by the high resource demands of conventional systems, making them unsuitable for small-scale robotic platforms which still require to perform complex, long-range tasks. Although neuromorphic approaches offer potential for greater efficiency, real-time edge deployment remains constrained by the complexity and limited scalability of bio-realistic networks. Here, we demonstrate a neuromorphic localization system that performs accurate place recognition in up to 8km of traversal using models as small as 180 KB with 44k parameters, while consuming less than 1% of the energy required by conventional methods. Our Locational Encoding with Neuromorphic Systems (LENS) integrates spiking neural networks, an event-based dynamic vision sensor, and a neuromorphic processor within a single SPECK™ chip, enabling real-time, energy-efficient localization on a hexapod robot. LENS represents the first fully neuromorphic localization system capable of large-scale, on-device deployment, setting a new benchmark for energy efficient robotic place recognition.

Introduction

Robot localization is an essential component of any autonomous navigation system, enabling robots to not only determine their location but also understand and interact with their surroundings. A central challenge in robot localization is visual place recognition (VPR), which requires robots to identify and classify previously visited locations under varying conditions (1–3). Conventional VPR strategies often rely on deep convolutional neural networks or transformer-based architectures to robustly extract features from the environment (4–7). For resource-constrained robotic platforms that nonetheless require the ability to keep track of where they are located over vast distances, using such conventional VPR methods is often not feasible due to their computational demands. An open challenge for real-world deployment of VPR is to find models that are computationally and energy efficient, and can be deployed at the edge.

Neuromorphic computing, which takes inspiration by the brain, has emerged as a promising solution for addressing the energy and computational challenges associated with robot localization and navigation (8–12). The human brain’s ability to learn and navigate complex environments efficiently (13–16) has inspired roboticists to create more compute efficient localization systems (17–21). In particular, Spiking Neural Networks (SNNs) have been widely explored due to their ability to perform tasks through bio-realistic simulations of neuron activity (22, 23). Whilst several SNN models have been proposed for robotic localization (10, 12, 24–32), they ultimately have not yet fully lived up to the promise of compute efficient deployment due to the complexity of continually modeling neurons in real-time (19, 24, 26).

To advance the practicality of neuromorphic computing in VPR, the focus must shift toward developing models that can be effectively deployed on Size, Weight, and Power (SWaP) constrained robotic platforms. One approach to overcoming deployment barriers is to trade the intricate bio-realism of traditional SNNs for simpler, more efficient networks that still deliver

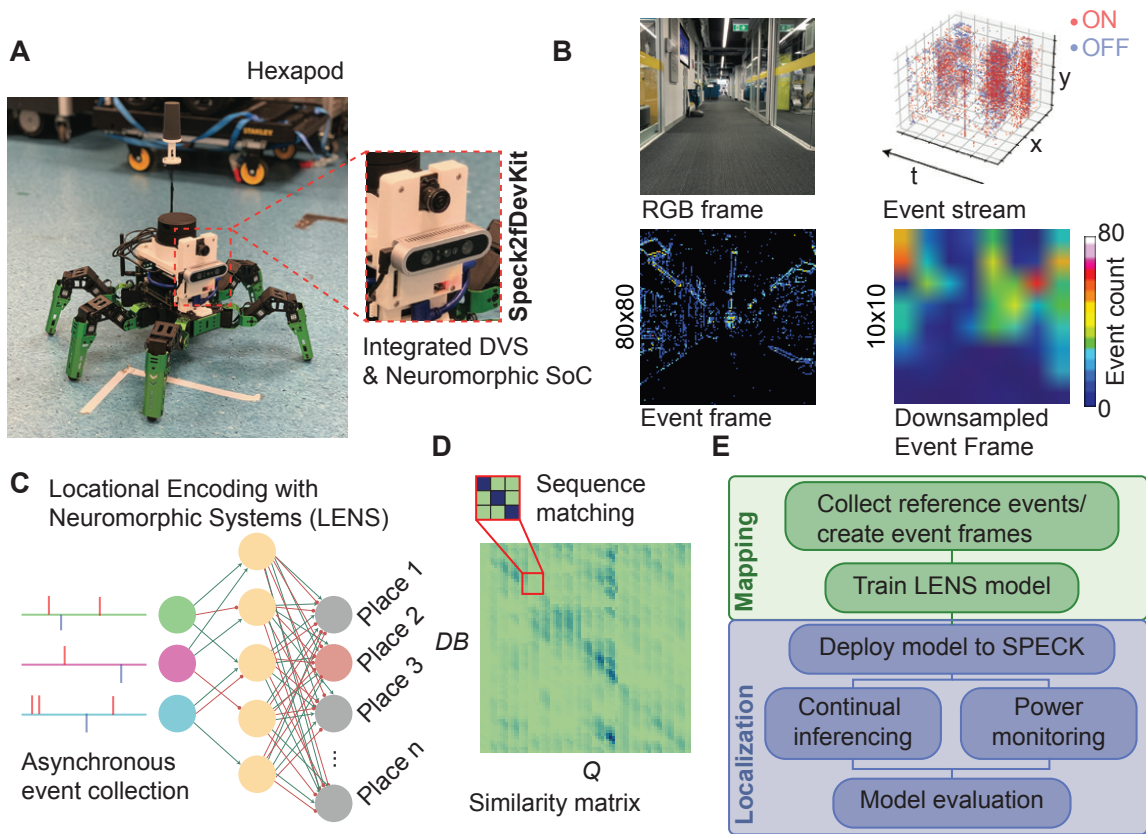


Figure 1: **Neuromorphic place recognition system on a hexapod robot.** Our system was deployed on a HiWonder Jetahexa hexapod robotic platform equipped with a custom 3D-printed mount housing a SynSense Speck2fDevKit (A). Event streams captured by the onboard DVS are processed into event frames by counting ON and OFF events during the hexapod’s traversal (B). The initial 128×128 input is cropped to a 80×80 region of interest which is then downsampled to 10×10 by selecting central pixels via a 2D convolutional layer (see Materials and Methods: Event processing). (C) The spiking neural network, Locational Encoding with Neuromorphic Systems (LENS), learns reference event frames for on-chip deployment, enabling real-time localization using asynchronously collected events. (D) Sequence matching techniques enhance the similarity between reference and query inputs, improving overall precision. (E) Schematic of the fully neuromorphic visual place recognition pipeline.

robust performance. However, these small-scale networks remain limited in their ability to map large environments, which restricts the downstream use-cases (11). To improve efficiency and scalability, SNNs full potential for robotic deployment can be realized by integrating them with neuromorphic hardware (10–12, 19, 33–36) such as Intel[®]'s Loihi 2, IBM's TrueNorth, and Tianjic (8, 37, 38), which draw inspiration from neuroscience for their design, enabling them to transmit and receive physical spikes from neurons within the processor cores (39).

Event cameras, including Dynamic Vision Sensors (DVS), offer further computational advantages when paired with neuromorphic processors as they only transmit information based on pixel-wise changes in light intensity exceeding a threshold, thereby reducing unnecessary data processing (34). Fusing neuromorphic algorithms, sensors, and processors to perform robotic localization tasks therefore provides a promising avenue to overcome the computational limitations inherent in SNN-based VPR (10, 12). While several neuromorphic localization systems have been developed and tested, they are limited by environment scale (11), require complex multi-modal fusion of large network models (12), or have restricted real-time capability (10).

Here, we introduce a novel neuromorphic pipeline for robotic localization that overcomes these limitations by enabling large-scale mapping and localization using a compact SNN with real-time performance. Our system, Locational Encoding with Neuromorphic Systems (LENS), is designed to deliver high accuracy and efficiency with a model size of less than 180 KB and 44K parameters, capable of processing up to 8 km of traversal data while consuming less than 1% of the energy required by conventional platforms. We train a temporally coded SNN designed to perform VPR (27) and deploy our model on the SynSense SPECK[™] (40), which combines a DVS and system-on-chip neuromorphic processor. By deploying on SPECK[™], we forgo the need for any external sensory modalities (e.g. satellites) or compute resources as all localization is performed on-chip. By abstracting complex bio-realism in favor of enhanced performance, LENS

represents a significant advancement in neuromorphic localization, as the first fully event-driven platform designed for VPR. We validate LENS on a HiWonder JetHexa hexapod robot (Fig. 1), demonstrating its effectiveness in both indoor and outdoor small-scale traversals (≈ 25 -40m, 50-80 places) and large-scale datasets (≈ 8 km, 600 places) (41), showcasing its potential for online VPR.

Results

Power and energy efficiency Neuromorphic computing platforms offer a significant advantage in terms of power and energy consumption when compared to traditional von Neumann hardware, particularly in tasks like Visual Place Recognition (VPR) where energy efficiency is crucial for long-term operation on battery-powered robots. We measured the power consumed by various components of the SPECK™ neuromorphic processor (Fig. 2) while performing VPR, recorded in the range of milliwatts (Fig. 2A). Notably, when the robot is stationary, the DVS generates very few events which results in further reductions in power consumption. To quantify the energy savings of LENS deployed on the SPECK™ processor relative to von Neumann hardware, we simulated event streams for VPR using our LENS model on an Intel® i7-9700K CPU and a NVIDIA Jetson Nano, which runs the hexapod (see Materials and Methods: Off-chip simulation of event streams and Power measurements). We used simulated experiments to avoid additional energy costs associated with converting events from SPECK™ to event streams used for CPU processing. After subtracting baseline CPU power use (see Fig. S2 and S3), we found that the SPECK™ consumed an average of 2.7 mW, which is just 0.5% and 0.02% of the power required by the Jetson Nano and Intel® CPU, respectively, to perform the same operations (Fig. 2B).

The overall energy consumption (the integral of power over time) of the SPECK™ was 327 mJ, with the Jetson using 9865 mJ and the Intel® CPU requiring 377,857 mJ, meaning overall our system required just 3.31% and 0.09% of the energy needed to perform the same task on von

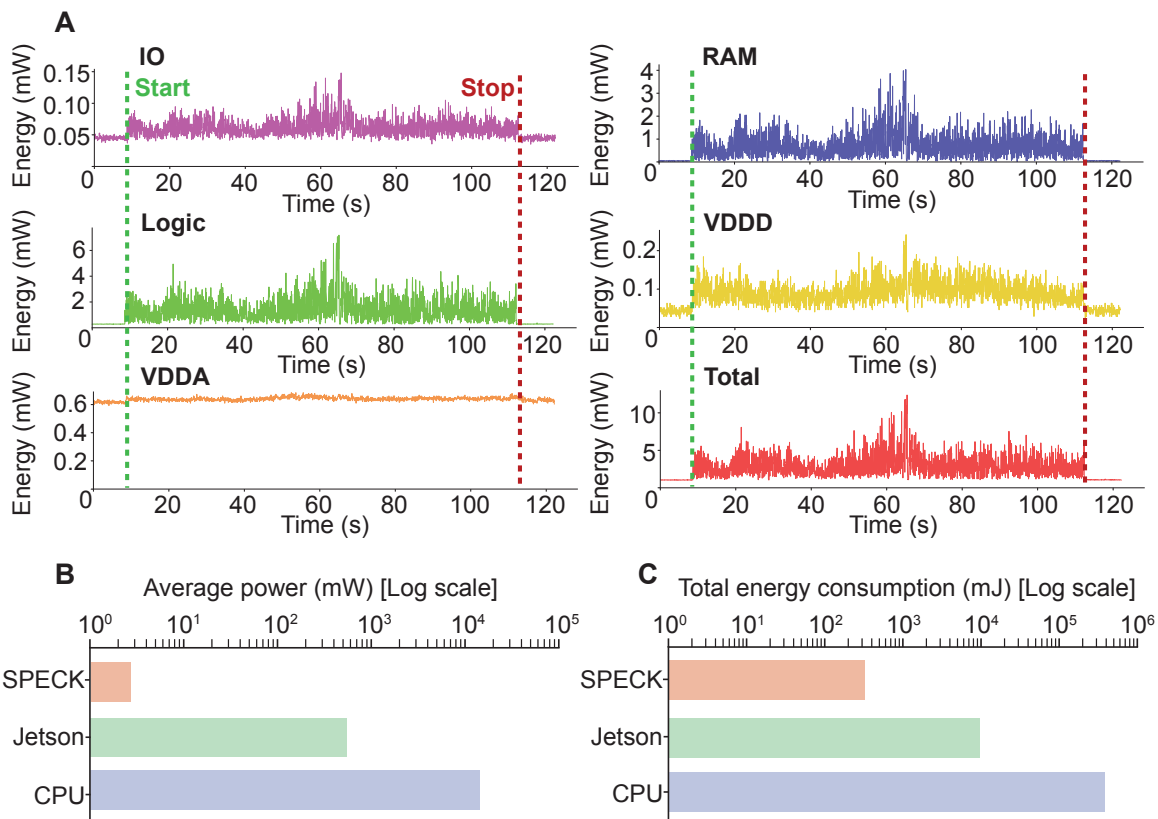


Figure 2: Energy efficiency of Real-time VPR on a neuromorphic processor vs. von Neumann hardware. (A) Power consumption was recorded across 5 components of the SPECK™ neuromorphic processor: input/output (IO), memory (RAM), logic, digital components (VDDD), analog components (VDDA), and the total. Start indicates when the robot began to move until the navigation task has finished, indicated by the Stop. (B) The average power consumption rates for the SPECK™, Jetson Nano, and Intel® CPU were 3 mW, 536 mW, and 13,696 mW, respectively. In the context of our VPR task in (A), the SPECK™ consumed significantly less total energy compared to the Jetson Nano and Intel® CPU, consuming 327 mJ, 9865 mJ, and 377,858 mJ, respectively (C). The mW and mJ values are presented on a logarithmic scale for display purposes.

Neumann hardware (Fig. 2C).

Localization performance during a navigation task To evaluate our system’s real-time performance, we performed VPR on our hexapod in both indoor and outdoor environments (Fig. 3). The model architecture was designed with $100 \times 200 \times 75$ for the input, feature, and output neurons, respectively. As illustrated in Figs. 3A & F, our generated event frames correspond to the environment being traversed, and particularly detect edges in the scene. The robot dealt with viewpoint and timing differences between the mapping and localization phases, as the route paths differed due to imperfect teleoperation (Figs. 3B & G). We used spikes from the model’s output layer to generate similarity matrices (Figs. 3C & H, see Materials and Methods: Online place matching). The similarity matrix was used to compute precision and recall metrics, which evaluates how well the robot is correctly identifying its location as it moves through the environment (Fig. 3C & H). We also employed the Sum-of-Absolute-Differences (SAD) method (42, 43) as a baseline comparison method, calculating pixel-wise similarity between mapping (training) and localization (test) data.

For the indoor task, LENS achieved a Recall@1 of 0.36, comparable to SAD’s performance at 0.35 (Fig. 3D). The precision-recall curve (PR-curve) indicated that LENS achieved higher precision at lower recall values compared to SAD (Fig. 3E), suggesting that LENS is highly accurate in its identification of places, even if it recognizes fewer places overall. In the outdoor task, however, SAD outperformed LENS with a Recall@1 of 0.17 and 0.15, respectively (Fig. 3I). SAD also achieved a higher precision at lower recall, shown in the PR-curve (Fig. 3J).

The reduced performance in outdoor environments is likely due to the higher dynamic range and higher incidence of non-static objects. As indicated by the similarity matrix (Fig. 3H), LENS showed a higher amount of activity across multiple output neurons. Fig. S1 suggests that increased contrastive differences in lighting during the navigation task introduced noise,

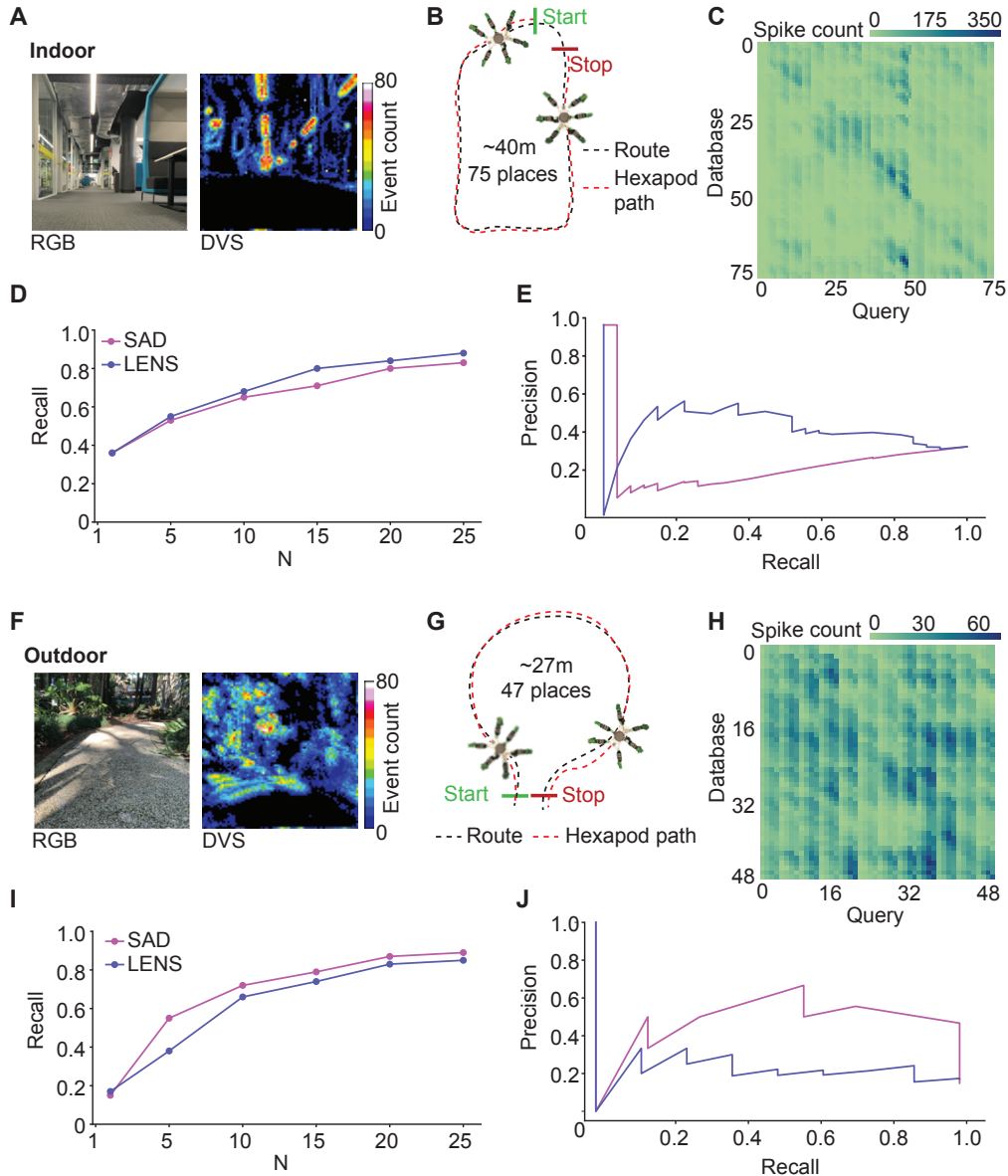


Figure 3: **Precision of a real-time neuromorphic robotic localization platform.** We deployed our robotic platform in two distinct areas, indoor (A) and outdoor (F), to compare how our system compares in different environments. Mapping and localization is performed through a predetermined route in each environment using the hexapod, with slight differences in viewpoint between the two datasets (B, G). To analyze the precision and recall of our model, we generated sequenced matched similarity matrices of the output spikes from all output neurons in our model while localizing (C, H). Our compact system performed comparably to the sum of absolute differences (SAD) method for Recall@N (D, I) and Precision-Recall (E, J), with LENS being better suited for indoor routes than outdoor.

distributing spikes across more neurons.

Overall, our compact spiking neural network model (130-150 KB in size) demonstrated comparable performance for VPR tasks in multiple environments, with key advantages of real-time deployability whilst being highly power and energy efficient. By contrast, the SAD method requires 388 KB to store the images, ≈ 2.6 times the storage space needed for our model. For scalable applications, our system offers clear benefits in terms of model size, making it feasible for deployment on resource-constrained compute platforms.

Large-scale place recognition with compact models To assess our system’s suitability for other real-world scenarios, we evaluated its performance in large scale environments using the Brisbane Event VPR dataset containing event streams from an ≈ 8 km route in Brisbane, Australia (41) (Fig. 4). This dataset circumvents limitations due to the hexapod’s low movement speed (see Materials and Methods: Robotic deployment). We generated 641 event frames of unique places by sampling over 1 second intervals from the dataset (Fig. 4B). To fit the model onto the SPECK™ chip, we adjusted the network architecture to 49 input neurons, 63 feature layer neurons, and 641 output neurons. This was the largest and highest performing model architecture we could use to run our model on-chip, balancing the number of input pixels and feature representation (Fig. S4). We used the “sunset2” traverse for mapping (reference dataset), and the “sunset1” traverse for localization (query dataset).

Both LENS and SAD generated similarity matrices that closely aligned with the ground truth (Fig. 4C). Although SAD outperformed LENS for Recall@N, achieving a Recall@1 of 0.63 compared to LENS’s 0.36 (Fig. 4D), LENS demonstrated better precision at lower recall, indicating higher confidence in its place recognition (Fig. 4E). However, we note that a spiking neural network achieving this degree of accuracy with an architecture of just 753 neurons across 3 layers shows promise for large scale place recognition applications. We required the same

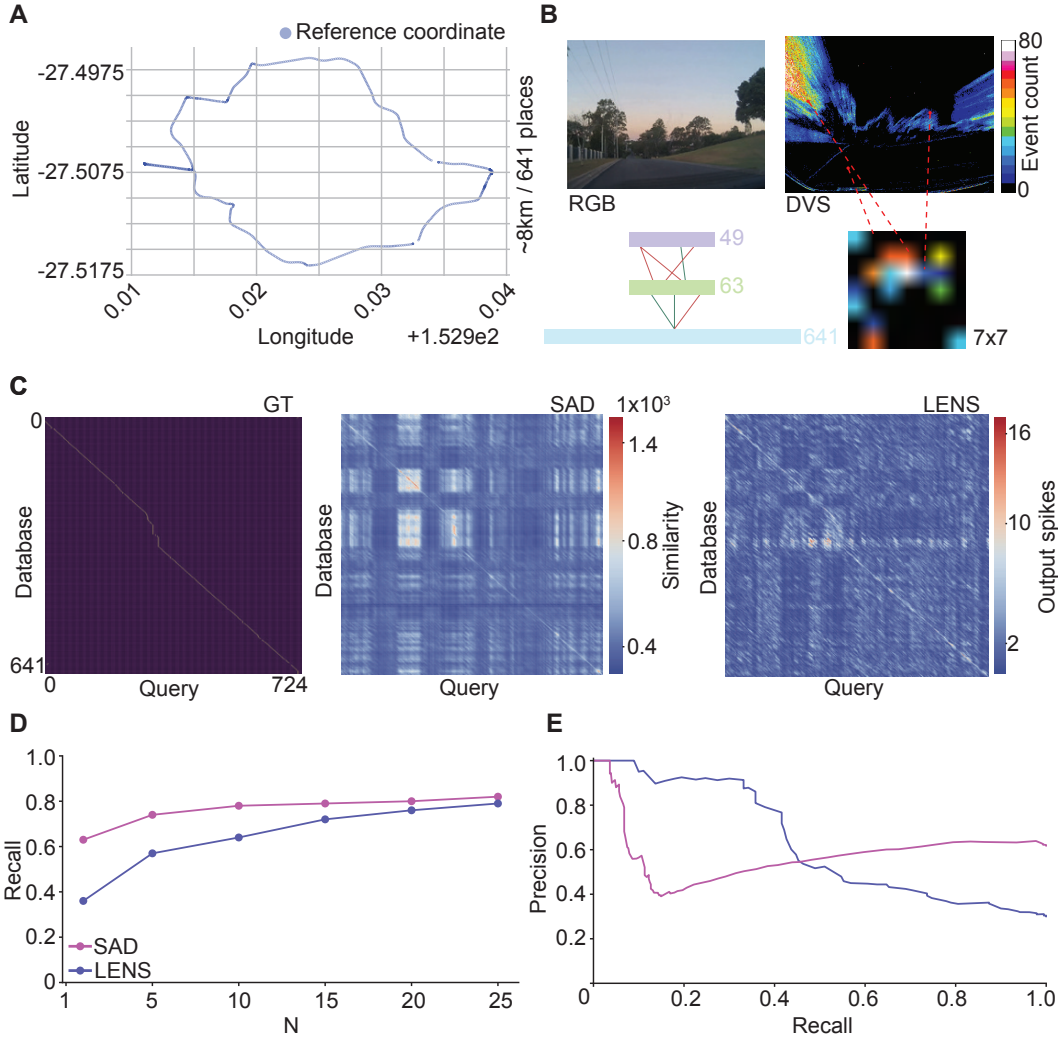


Figure 4: **Large scale place recognition using a compact neuromorphic ecosystem.** (A) Coordinate map of the Brisbane Event VPR dataset route (41) which represents an ≈ 8 km traversal and 641 unique place locations around the suburbs of Brisbane, Australia. (B) Event frames are generated in the same way as on robot experiments (Fig. 3). Pixels were selected randomly rather than applying a 2D convolutional filter due to a larger event camera resolution used in (41). We selected pixels to generate event frames that are 7×7 in size. Our model architecture was modified to $49 \times 63 \times 641$ to allow for on-chip inferencing. (C) Similarity matrices for both SAD and LENS, showing how the similarity for both methods aligns closely with the ground truth (GT). (D) Recall@N and (E) Precision-Recall curves for our method when compared to SAD. SAD performed better at Recall@1 with 0.63 compared to ours at 0.36, however we achieved better precision at lower recall indicating our system is more confident at the places it selected. The energy efficiency and compact model size of just 753 neurons with 44K parameters highlights the benefit of our system.

amount of storage space capacity to store our model and the down sampled images for SAD, which was ≈ 179 KB. If memory constraints on SPECKTM had not been a limiting factor, larger LENS networks could perform as well or better than SAD (Fig. S4). For example, a model architecture of $49 \times 98 \times 641$ input, feature, and output neurons respectively measures at just 278 KB and performs comparably to SAD (Fig. S4).

Interestingly, both SAD and LENS performed better on the Brisbane Event VPR dataset than during the on-robot VPR task (Fig. 3). The Brisbane Event Dataset utilized a 346×240 sensor (41), compared to the 128×128 sensor (44) on our robot. Additionally, the more stable platform (i.e., a car) used for dataset collection could reduce errors from viewpoint variance or swaying movement observed with the hexapod (see Movie 1). These results indicate that our proposed model can be effectively deployed in various environments and on different robotic platforms for a wide range of localization and navigation tasks.

Discussion

This work demonstrated a fully neuromorphic visual place recognition system capable of real-time localization, which was successfully deployed on a hexapod robotic platform without any external sensing or compute resources. The LENS spiking neural network model, characterized by its simplicity and compactness, performed accurately across multiple environments and scales, demonstrating its versatility for a range of navigation platforms and tasks. Our system integrated with the SPECKTM chip operated with three orders of magnitude lower energy than conventional von Neumann computing platforms, underscoring its viability for deployment on resource-constrained platforms such as unmanned aerial vehicles (45), underwater (46), and locomotive robotics (47).

Notably, our models were less than 180 KB in size, with the largest containing just 44k parameters. Accurate localization with compact models enables scalability, particularly with

deployment on neuromorphic processors with higher memory capability for larger models (Fig. S4). Previous research has shown that accurate place recognition with event cameras can be achieved with as few as 25 pixels (42). Our system capitalized on this by expanding the feature representation of event pixels, rather than increasing pixel count, to enhance performance (Fig. S4). A limiting factor in this work was the memory capacity of the neurocores for SPECK™, which cap at 64 KB per core. Overcoming this limitation with neuromorphic hardware offering higher memory capabilities could further enhance the performance of large-scale place recognition tasks (Fig. S4). Nonetheless, we have shown comparable performance for place recognition in highly compact spiking network models across multiple environments.

As observed in the comparison between indoor and outdoor localization tasks (Fig. 3), higher dynamic ranges proved challenging for LENS. Future work should focus on dynamically adjusting the biases and parameters of DVS event streams to better handle changes in lighting conditions (48). Additionally, the turning motions of the hexapod proved challenging for LENS, as rotations triggered widespread activation across the DVS field of view, potentially introducing noise while localizing. This issue was particularly pronounced in outdoor tasks, where the navigation route involved more turns than the indoor path. Continued development of this system will focus on detecting and handling turning motions to for improved localization performance.

Another limitation of our system is the use of static, temporally framed representations generated from event streams without temporal binning for model training. Training our model directly on DVS event streams could help overcome the localization challenges observed in dynamic environments. Developing this would also lend itself for online learning capabilities, where event streams are used directly to train network models in real-time. This would enable the system to adapt to new environments on-the-go, potentially incorporating introspective capabilities that allow the robot to recognize when it is uncertain about its location and learn accordingly (49–52).

Materials and Methods

Event processing The Locational Encoding with Neuromorphic Systems (LENS) framework leverages spiking neural networks (SNN) on neuromorphic processors for computationally and energy efficient place recognition. We deployed our SNN model on a SynSense Speck2fDevKit, which incorporates the SPECK™ neuromorphic processor with a 128×128 dynamic vision sensor (DVS) (40) for event driven, real-time localization.

To optimize input size and remove low-activity pixels, we first select an 80×80 region of interest (ROI) in the top-center of the sensor. Events from this ROI were processed using a 2D convolution layer with a kernel size and stride of 8. We set the center weight of the kernel to 1, with all other weights at 0, effectively selecting the center pixel from each convolution to reduce the input to 100 neurons. This selection approach follows a previously established method for event pixel selection (42).

The input neurons were sparsely connected to a linear feature layer of 200 neurons, with excitatory and inhibitory connection probabilities set at 10% and 50% respectively. The feature layer was fully connected to the output layer, with the number of output neurons corresponding to the number of learnt places (see Materials and Methods: Model training). Pre-processed events were asynchronously collected and passed into our model, where Constant-leak Integrate and Fire (IAF) neurons propagated spikes across the network layers:

$$\tau \dot{v} = -v_{\text{leak}} + R \cdot (I_{\text{syn}} + I_{\text{bias}}), \quad (1)$$

where τ is the membrane time constant, v is the membrane potential, R is the constant resistance value used to match units between membrane potential and currents, I_{syn} is the weighted sum of all input synaptic contributions, and I_{bias} is a constant bias.

Model training Our network models were trained using temporal representations of event streams, normalized in the range $[0, 1]$ and encoded using a time-to-first spike coding scheme (53). The network was trained based on the temporal dynamics of the spike-timing (27, 54). The 3-layer architecture (input, feature, and output) used unsupervised learning between the input and feature layers, and a supervised delta learning rule for the feature to output layer.

Unsupervised learning applied spike-timing dependent plasticity (STDP) to update weights W , encouraging or pruning connections between neurons. Connections can be positive (*excitatory connection*) or negative (*inhibitory connection*):

$$\Delta W_{ji}^{nm}(t) = \frac{\eta_{\text{STDP}}(t)}{f_j^n} \cdot \left[\Theta(x_i^m(t-1)) \cdot \Theta(x_j^n(t)) \cdot (0.5 - x_j^n(t)) \right], \quad (2)$$

where W_{ij}^{nm} is the connection weight between neuron j in layer n to neuron i in layer m , η_{STDP} is the STDP learning rate, f_j^n is the target firing rate of neuron j in layer n , $\Theta(\cdot)$ is the Heaviside step function, x_i^m and x_j^n are the pixel intensity spike values of pre- or post-synaptic neurons respectively, and t is the timestep.

For supervised learning between the feature and output layer, we employed a delta learning rule to force each output neuron to learn the feature representation of a single reference place (27, 54):

$$\Delta W_{ji}^{nm}(t) = \eta_{\text{STDP}}(t) / f_j^n \cdot [x_i^m(t-1)(x_{\text{force } j}^n(t) - x_j^n(t))], \quad (3)$$

where x_{force} is the forced spike in the selected output neuron during training.

The hyperparameters used for our models can be found in Table S1 which were obtained by performing a random hyperparameter sweep search.

Online place matching Place matching was performed using real-time sequence matching (43, 55) to enhance the precision of our VPR model on the SPECKTM. Spike counts from the output layer were collected in 1-second time bins, then averaged over 4 time bins (4 seconds), representing ≈ 0.5 m of robot movement (average speed of $13.5 \text{ cm} \cdot \text{s}^{-1}$). Once 4 sets of output spike counts were gathered, representing about 2 m of travel, they were compiled into a distance matrix M_{dist} , which was convolved with an identity matrix \mathbb{I} to generate a sequence-based distance matrix M_{seq} , as previously described (55):

$$M_{seq}(i, j) = \mathbb{I} * M_{dist}(i, j) / L. \quad (4)$$

where i and j are the row and column of the matrix, respectively, and L is the sequence length, which we set to 4 matching the number of output spike counts.

The matched place \hat{p} was identified as the place i corresponding to the neuron with the highest spike count x_i :

$$\hat{p} = \arg \max_i x_i. \quad (5)$$

Off-chip simulation of event streams For power and energy consumption comparisons, we simulated event-driven inference using event frames from the SPECKTM energy experiments (see Materials and Methods: Power and energy measurements). Integrate And Fire neuron spike rates were generated using a time-based rate code:

$$I_{t,h,w} = \begin{cases} 1 & \text{if } R_{t,h,w} < X_{h,w} \\ 0 & \text{otherwise,} \end{cases} \quad (6)$$

where $I_{t,h,w}$ is a boolean tensor with spatial dimensions h and w over t time-windows, where 1 = spike and 0 = no spike. $R_{t,h,w} \in [0, 1]$ is a uniformly random tensor, and $X_{h,w}$ is the

original input. Inference was simulated over 1000 time windows with $dt = 0.001s$ to represent 1s of output spike collection, similar to the online place matching (see Materials and Methods: Online place matching).

Robotic deployment We used the commercially available JetHexa hexapod (Hiwonder, Shenzhen China) customized with a 3D-printed mount to house the Speck2fDevKit (see Fig. 1). Training data was collected by teleoperating the robot for a reference traversal. Real-time localization was performed on the SPECK™ neuromorphic processor with the pre-trained model closely following the reference traversal. Indoor and outdoor datasets represented approximately 40m and 27m of traversal, encoding 75 and 48 unique places, respectively. To ensure accurate ground truth alignment between the mapping and localization phases, experiments were consistently started and ended at the same location.

Power and energy measurements Intel® CPU power was measured using SoC Watch (Fig. S2), and NVIDIA Jetson Nano power was recorded with the jetson-stats Python package (Fig. S3), with baseline idle power subtracted in both cases. SPECK™ power tracks (IO, RAM, memory, VDDA, and VDDD) were recorded at 20 Hz using the samna package during testing (see Movie 1 and Fig. 2).

Statistical analysis We evaluate our system using Recall@N and precision-recall curves, two standard metrics for VPR studies (*I*). Recall@N measures the accuracy of the system such that for $N = 1$ only the highest match is considered, whereas for $N = 5$ the top 5 matches are considered when calculating the accuracy. We used the Sum of Absolute Differences (SAD) method for comparison, which computes pixel-wise similarity across reference and query images and has been used previously for place recognition using event streams (*42, 43*). We allow a ground-truth tolerance of $\approx 1m$, which is equivalent to ± 2 reference places.

Code and data availability To foster future research and development, we have made the code and data for our SNN and its robotic deployment available at:

<https://github.com/AdamDHines/LENS>

References

1. S. Schubert, P. Neubert, S. Garg, M. Milford, T. Fischer, Visual place recognition: A tutorial, *IEEE Robotics and Automation Magazine* (2023).
2. X. Zhang, L. Wang, Y. Su, Visual place recognition: A survey from deep learning perspective, *Pattern Recognition* **113**, 107760 (2021).
3. C. Masone, B. Caputo, A survey on deep visual place recognition, *IEEE Access* **9**, 19516 (2021).
4. G. Berton, C. Masone, B. Caputo, Rethinking visual geo-localization for large-scale applications, *IEEE/CVF Conference on Computer Vision and Pattern Recognition* (2022).
5. G. Neuhold, T. Ollmann, S. R. Bulò, P. Kotschieder, The mapillary vistas dataset for semantic understanding of street scenes, *IEEE International Conference on Computer Vision* (2017).
6. M. Cordts, *et al.*, The cityscapes dataset for semantic urban scene understanding, *Proceedings of the IEEE/CVF Conference on Computer Vision and Pattern Recognition* (2016).
7. S. Izquierdo, J. Civera, Optimal transport aggregation for visual place recognition, *Proceedings of the IEEE/CVF Conference on Computer Vision and Pattern Recognition* (2024).
8. G. Orchard, *et al.*, Efficient neuromorphic signal processing with Loihi 2, *IEEE Workshop on Signal Processing Systems* (2021).

9. E. Painkras, *et al.*, SpiNNaker: A multi-core system-on-chip for massively-parallel neural net simulation, *IEEE Custom Integrated Circuits Conference* (2012).
10. L. Zhu, M. Mangan, B. Webb, Neuromorphic sequence learning with an event camera on routes through vegetation, *Science Robotics* **8** (2023).
11. T. van Dijk, C. D. Wagter, G. C. H. E. de Croon, Visual route following for tiny autonomous robots, *Science Robotics* **9** (2024).
12. F. Yu, *et al.*, Brain-inspired multimodal hybrid neural network for robot place recognition, *Science Robotics* **8** (2023).
13. K. Friston, The free-energy principle: a unified brain theory?, *Nature Reviews Neuroscience* **11** (2010).
14. D. Chen, N. Axmacher, L. Wang, Grid codes underlie multiple cognitive maps in the human brain, *Progress in Neurobiology* **233** (2024).
15. J. E. Lisman, O. Jensen, The Theta-Gamma neural code, *Neuron* **77** (2013).
16. C. Liu, R. Todorova, W. Tang, A. Oliva, A. Fernandez-Ruiz, Associative and predictive hippocampal codes support memory-guided behaviors, *Science* **382** (2023).
17. M. J. Milford, G. F. Wyeth, Mapping a suburb with a single camera using a biologically inspired SLAM system, *IEEE Transactions on Robotics* **24** (2008).
18. F. Yu, J. Shang, Y. Hu, M. Milford, NeuroSLAM: a brain-inspired SLAM system for 3D environments, *Biological Cybernetics* **113** (2019).
19. J. Wang, S. Lin, A. Liu, Bioinspired perception and navigation of service robots in indoor environments: A review, *Biomimetics* **8** (2023).

20. L. Wang, S. X. Yang, M. Biglarbegian, Bio-inspired navigation of mobile robots, *Autonomous and Intelligent Systems* (2012).
21. T. Joseph, T. Fischer, M. Milford, Trajectory tracking via multiscale continuous attractor networks, *IEEE/RSJ International Conference on Intelligent Robots and Systems* (2023).
22. A. Tavanaei, M. Ghodrati, S. R. Kheradpisheh, T. Masquelier, A. Maida, Deep learning in spiking neural networks, *Neural Networks* **111** (2019).
23. J. K. Eshraghian, *et al.*, Training spiking neural networks using lessons from deep learning, *Proceedings of the IEEE* **111** (2023).
24. S. Hussaini, M. Milford, T. Fischer, Ensembles of compact, region-specific & regularized spiking neural networks for scalable place recognition, *IEEE International Conference on Robotics and Automation* (2023).
25. S. Hussaini, M. J. Milford, T. Fischer, Spiking neural networks for visual place recognition via weighted neuronal assignments, *IEEE Robotics and Automation Letters* **7** (2022).
26. S. Hussaini, M. Milford, T. Fischer, Applications of spiking neural networks in visual place recognition, *arXiv* (2023).
27. A. D. Hines, P. G. Stratton, M. Milford, T. Fischer, Vprtempo: A fast temporally encoded spiking neural network for visual place recognition, *IEEE International Conference on Robotics and Automation* (2024).
28. N. S. Giraldo, S. Isaza, R. A. Velásquez, Sailboat navigation control system based on spiking neural networks, *Control Theory and Technology* (2023).
29. J. Liu, H. Lu, Y. Luo, S. Yang, Spiking neural network-based multi-task autonomous learning for mobile robots, *Engineering Applications of Artificial Intelligence* **104** (2021).

30. G. Tang, A. Shah, K. P. Michmizos, Spiking neural network on neuromorphic hardware for energy-efficient unidimensional SLAM, *IEEE/RSJ International Conference on Intelligent Robots and Systems* (2019).
31. F. Galluppi, *et al.*, Live demo: Spiking ratSLAM: Rat hippocampus cells in spiking neural hardware, *IEEE Biomedical Circuits and Systems Conference* (2012).
32. G. qiang Bi, M. ming Poo, Synaptic modifications in cultured hippocampal neurons: Dependence on spike timing, synaptic strength, and postsynaptic cell type, *Journal of Neuroscience* **18** (1998).
33. C. Bartolozzi, G. Indiveri, E. Donati, Embodied neuromorphic intelligence, *Nature Communications* **13** (2022).
34. G. Gallego, *et al.*, Event-based vision: A survey, *IEEE Transactions on Pattern Analysis & Machine Intelligence* **44** (2022).
35. N. Russo, H. Huang, E. Donati, T. Madsen, K. Nikolic, An interface platform for robotic neuromorphic systems, *Chips* **2** (2023).
36. Y. Yang, C. Bartolozzi, H. H. Zhang, R. A. Nawrocki, Neuromorphic electronics for robotic perception, navigation and control: A survey, *Engineering Applications of Artificial Intelligence* **126** (2023).
37. F. Akopyan, *et al.*, TrueNorth: design and tool flow of a 65 mw 1 million neuron programmable neurosynaptic chip, *IEEE Transactions on Computer-Aided Design of Integrated Circuits and Systems* **34** (2015).
38. J. Pei, *et al.*, Towards artificial general intelligence with hybrid tianjic chip architecture, *Nature* **572** (2019).

39. B. J. Shastri, *et al.*, Principles of neuromorphic photonics, *Encyclopedia of Complexity and Systems Science* (2018).
40. M. Yao, *et al.*, Spike-based dynamic computing with asynchronous sensing-computing neuromorphic chip, *Nature Communications* **15** (2024).
41. T. Fischer, M. Milford, Event-based visual place recognition with ensembles of temporal windows, *IEEE Robotics and Automation Letters* **5** (2020).
42. T. Fischer, M. Milford, How many events do you need? event-based visual place recognition using sparse but varying pixels, *IEEE Robotics and Automation Letters* **7** (2022).
43. M. J. Milford, G. F. Wyeth, SeqSLAM: visual route-based navigation for sunny summer days and stormy winter nights, *IEEE International Conference on Robotics and Automation* (2012).
44. P. Lichtsteiner, C. Posch, T. Delbruck, A 128×128 120 db 15 μ s latency asynchronous temporal contrast vision sensor, *IEEE Journal of Solid-State Circuits* **43**, 566 (2008).
45. S. Bian, *et al.*, Colibriuav: An ultra-fast, energy-efficient neuromorphic edge processing uav-platform with event-based and frame-based cameras, *IEEE International Workshop on Advances in Sensors and Interfaces* (2023).
46. E. Kelasidi, K. Y. Pettersen, J. T. Gravdahl, Energy efficiency of underwater robots, *IFAC Conference on Manoeuvring and Control of Marine Craft* **48** (2015).
47. N. Kashiri, *et al.*, An overview on principles for energy efficient robot locomotion, *Frontiers in Robotics and AI* **5** (2018).

48. G. B. Nair, M. Milford, T. Fischer, Enhancing visual place recognition via fast and slow adaptive biasing in event cameras, *IEEE/RSJ International Conference on Intelligent Robots and Systems* (2024).
49. Y. Wu, *et al.*, Brain-inspired global-local learning incorporated with neuromorphic computing, *Nature Communications* **13** (2022).
50. R. Zhu, *et al.*, Online dynamical learning and sequence memory with neuromorphic nanowire networks, *Nature Communications* **14** (2023).
51. A. Rostami, B. Vogginger, Y. Yan, C. G. Mayr, E-prop on spinnaker 2: Exploring online learning in spiking rnns on neuromorphic hardware, *Frontiers in Neuroscience* **16** (2022).
52. S. Hwang, *et al.*, Replacenet: real-time replacement of a biological neural circuit with a hardware-assisted spiking neural network, *Frontiers in Neuroscience* **17** (2023).
53. W. Guo, M. E. Fouda, A. M. Eltawil, K. N. Salama, Neural coding in spiking neural networks: A comparative study for robust neuromorphic systems, *Frontiers in Neuroscience* **15** (2021).
54. P. G. Stratton, A. Wabnitz, C. Essam, A. Cheung, T. J. Hamilton, Making a spiking net work: Robust brain-like unsupervised machine learning, *arXiv 2208.01204* (2022).
55. S. Garg, M. Vankadari, M. Milford, Seqmatchnet: Contrastive learning with sequence matching for place recognition & relocalization, *Conference on Robot Learning* (2022).

Acknowledgments

This work received funding from an ARC Laureate Fellowship FL210100156 to MM and AUS-MURIB000001 associated with ONR MURI grant N00014191-2571. The authors acknowledge

continued support from the Queensland University of Technology (QUT) through the Centre for Robotics. We wish to acknowledge the support of the Research Engineering Facility (REF) team at QUT for the provision of engineering support, expertise and research infrastructure in enablement of this project. We also would like to thank Dr Scarlett Raine and Dr Somayeh Hussaini for their valuable feedback during manuscript preparation. Finally, we would like to thank the organisers and participants of the 2022 Lifelong Learning at Scale topic area at the Telluride Neuromorphic Workshop for the insightful discussions and inspiring environment, which helped shape some of the ideas explored in this paper.

Supplementary materials

Figure S1

Figure S2

Figure S3

Figure S4

Table S1

Movie 1

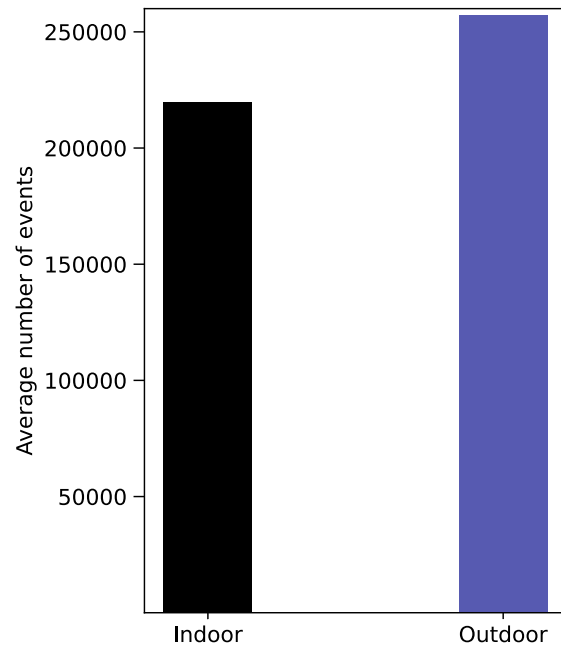


Figure S1: Average number of events between indoor and outdoor traversals.

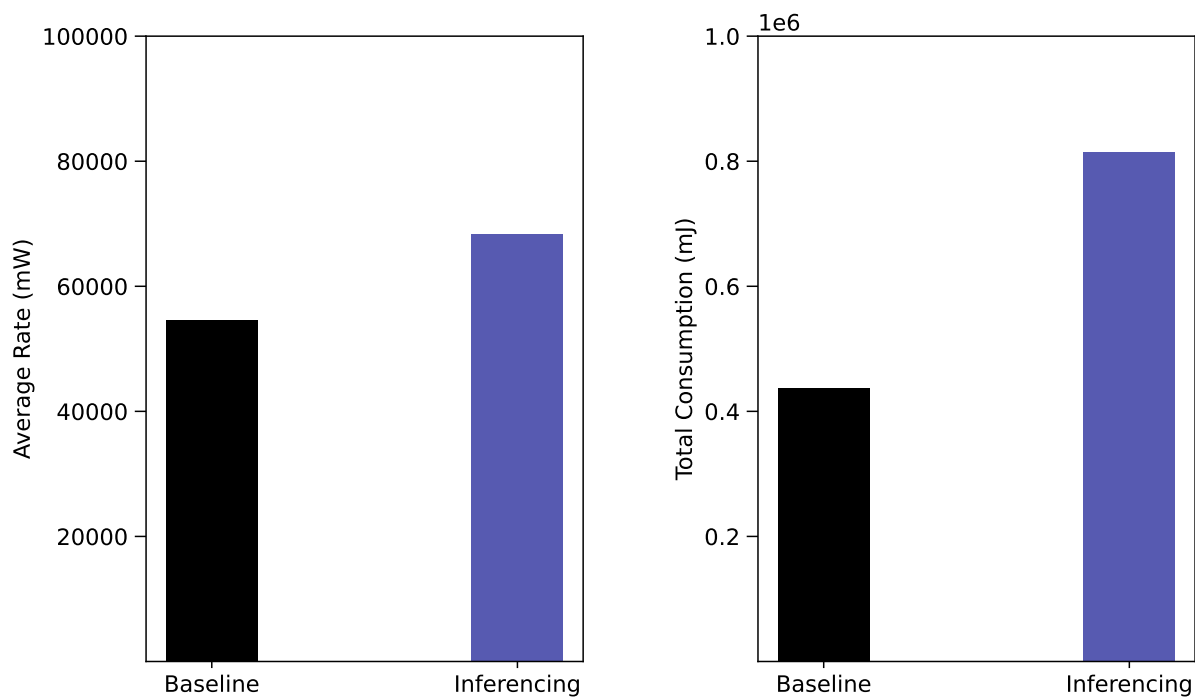


Figure S2: **Power and energy measurements for our Intel® CPU experiment.** The baseline power consumption and energy was subtracted using the SoC Watch software from the inferencing measurements for our comparisons to other hardware.

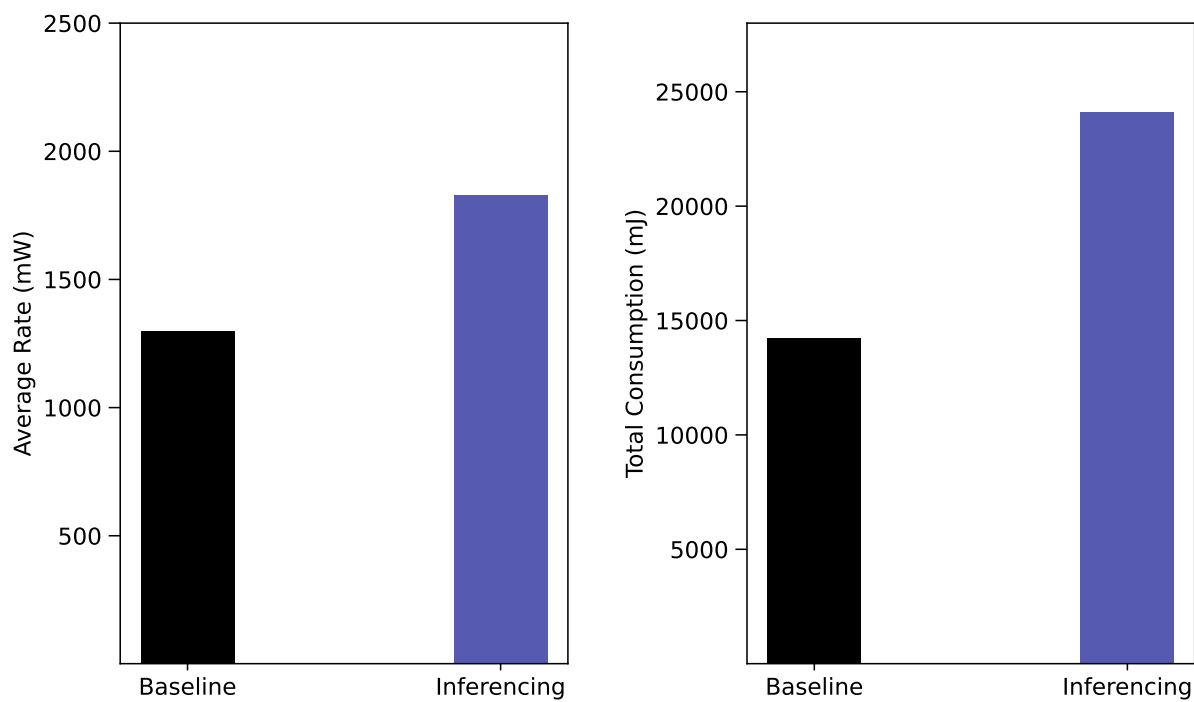


Figure S3: **Power and energy measurements for our Jetson Nano experiment.** The baseline power consumption and energy measured with the jetson-stats package was subtracted from the inferencing measurements for our comparisons to other hardware.

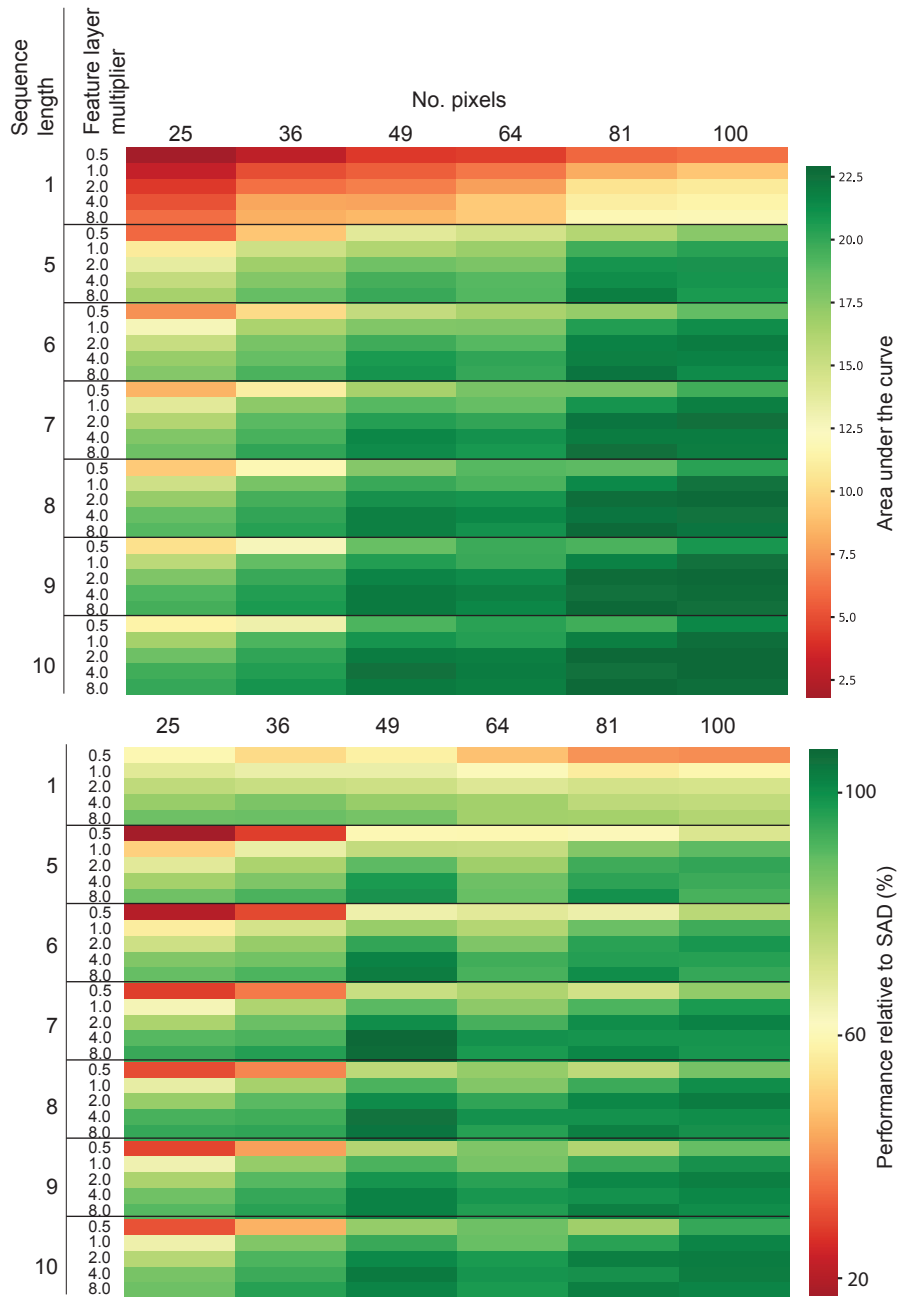


Figure S4: **Effects of model size and sequence length on network performance.** (Top) Heatmap of the area under the curve of the Recall@N results from training and testing the Brisbane Event VPR data (41) for different number of input pixels, feature layer size multiplier (relative to number of pixels), and sequence lengths. Our model with $49 \times 49 \times 641$ neurons with a sequence length of 10 was the highest performer whilst still being able to be deployed to SPECK™. The best performing model had the architecture of $100 \times 200 \times 641$ neurons and a sequence length of 10, indicating that model accuracy heavily depends on the number of input events the ratio of the feature layer to the input (Bottom). Performance of the various models relative to sum of absolute differences for the area under the curve.

Table S1: Hyperparameters for network training

Parameter	$\theta_{\max}^{I \rightarrow F}$	$\theta_{\max}^{F \rightarrow O}$	$\eta_{\text{STDP}}^{\text{init}}$	$\eta_{\text{ITP}}^{\text{init}}$	$f_{\min}^{I \rightarrow F}, f_{\max}^{I \rightarrow F}$	$f_{\min}^{F \rightarrow O}, f_{\max}^{F \rightarrow O}$
Values	0.75	0.5	0.01	0.02	[0.4, 0.6]	[0.5, 0.5]
Parameter	$P_{\text{exc}}^{I \rightarrow F}$	$P_{\text{inh}}^{I \rightarrow F}$	$P_{\text{exc}}^{F \rightarrow O}$	$P_{\text{inh}}^{F \rightarrow O}$	$\epsilon^{I \rightarrow F}$	$\epsilon^{F \rightarrow O}$
Values	0.1	0.5	1.0	1.0	128	128